

LETTER

Rietveld structure refinement of perovskite and post-perovskite phases of NaMgF₃
(Neighborite) at high pressures

C. DAVID MARTIN,^{1,*} WILSON A. CRICHTON,² HAOZHE LIU,³ VITALI PRAKAPENKA,⁴ JIUHUA CHEN,¹
AND JOHN B. PARISE^{1,5}

¹Geosciences Department, 255 Earth and Space Sciences Building, Stony Brook University, Stony Brook, New York 11794-2100, U.S.A.

²ID-27 European Synchrotron Radiation Facility (ESRF), 6 rue Jules Horowitz, BP220, 38043 Grenoble CEDEX, France

³High Pressure Collaborative Access Team (HP-CAT), Sector 16, Advanced Photon Source, Argonne National Laboratory, Argonne, Illinois 60439, U.S.A.

⁴GeoSoil and EnviroCARS (GSECARS), Sector 13, Advanced Photon Source, Argonne National Laboratory, Argonne, Illinois 60439, U.S.A.

⁵Chemistry Department, Stony Brook University, Stony Brook, New York 11794-3400, U.S.A.

ABSTRACT

Neighborite (NaMgF₃) with the perovskite structure, transforms to a post-perovskite (ppv) phase between 27 and 30 GPa. The ppv phase is observed to the highest pressures achieved (56 GPa) at room temperature and transforms to an as yet unknown phase upon heating. Rietveld structure refinement using monochromatic synchrotron X-ray diffraction data provide models for the perovskite and post-perovskite structures at high pressure. The refined models at 27(1) GPa indicate some inter-octahedral F-F distances rival the average intra-octahedral distance, which may cause instability in the perovskite structure and drive the transformation to the post-perovskite phase. The ratio of A-site to B-site volume (V_A/V_B) in perovskite structured NaMgF₃ (ABX₃), spans from 5 in the zero-pressure high-temperature cubic perovskite phase to 4 in this high-pressure perovskite phase at 27(1) GPa, matching the V_A/V_B value in post-perovskite NaMgF₃. Using Rietveld refinement on post-perovskite structure models, we observe discrepancies in pattern fitting, which may be described in terms of development of sample texture in the diamond-anvil cell, recrystallization, or a change of space group to *Cmc*2₁, a non-isomorphic subgroup of *Cmcm*—the space group describing the structure of CaIrO₃.

Keywords: Perovskite, post-perovskite, pressure, diamond anvil cell, X-ray diffraction, Rietveld modeling, structure

INTRODUCTION

At the lowermost region of Earth's mantle, the D'' layer (Dziewonski and Anderson 1981) is the medium through which heat and chemistry from the core may contact the mantle above. As a result, D'' is a complex boundary region (Lay et al. 2004), laterally variable and marked by seismic anomalies. Researchers have long sought to understand the origin and dynamics of this distinct layer (Karato and Karki 2001; Lay et al. 1998). Many high-pressure experiments have investigated MgSiO₃ perovskite for explanations to anomalous seismic phenomena observed in D'' and recent experiments have uncovered a post-perovskite structure of MgSiO₃ at pressures and temperatures thought to exist at D'' (Murakami et al. 2004; Oganov and Ono 2004).

A perovskite (pv) post-perovskite (ppv) transformation is reported to occur in several ABX₃ materials: MgGeO₃ (Hirose et al. 2005), CaIrO₃ (Hirose and Fujita 2005), and others (Tateno et al. 2006). In addition, the ppv structure is reportedly adopted in A₂X₃ materials Fe₂O₃ (Ono and Ohishi 2005), and Mn₂O₃ (Santillan and Shim 2005). The ppv structure is based on the CaIrO₃ model, which is orthorhombic (*Cmcm*, *Z* = 4), and rarely adopted among oxides and sulfides at room pressure. The CaIrO₃ structure (Rodi and Babel 1965) may be summarized as alternating layers of BX₆ octahedra and A-site cations normal to the *b* axis within a C-centered lattice (Fig. 1a). Octahedra share edges along the *a*

axis and corners along the *c* axis. The significant anisotropy of a CaIrO₃-type MgSiO₃ structure may explain the zones of strong seismic anisotropy observed within the D'' layer (Garnero 2004; Murakami et al. 2004; Tsuchiya et al. 2004).

The post-perovskite structure is now under intense study (Caracas and Cohen 2005; Mao et al. 2006; Murakami et al. 2005; Shieh et al. 2006) and debate. However, Rietveld structure modeling of ppv-MgSiO₃ is not yet documented. Powder statistics of X-ray diffraction data collected from samples in excess of 120 GPa are often compromised due to small scattering volumes present during experiments. Rietveld refinement of ppv structure will confirm the accuracy of the CaIrO₃ (*Cmcm*) model and the study of analog materials at extreme conditions is an alternative route to this goal. Analogs, such as MgGeO₃ (Duffy et al. 2005; Hirose and Fujita 2005), transform at lower pressures, increasing sample size, peak-to-background discrimination, and overall data quality.

The structure of neighborite (NaMgF₃) (Chao et al. 1961) was recently studied as an analog material for pv MgSiO₃ (O'Keefe et al. 1979) using Rietveld structure modeling (Martin et al. 2005; Zhao et al. 1993). Previous work (Liu et al. 2005; Martin et al. 2006) finds a pv-ppv phase transition in NaMgF₃ between 28 and 30 GPa, in agreement with enthalpy calculations (Parise et al. 2004).

Previously we have reported the high-pressure phase transformations of NaMgF₃ (Martin et al. 2006). In the following letter, we report results of Rietveld refinement, detailing the high-pressure perovskite and post-perovskite structures of

* E-mail: chmartin@ic.sunysb.edu

NaMgF₃. From our analysis we reveal a high-pressure instability in the pv-NaMgF₃ structure and test the CaIrO₃ (*Cmcm*) structure model of ppv-NaMgF₃.

EXPERIMENTAL METHODS

Synthetic NaMgF₃ was prepared according to published procedure (Zhao et al. 1993). Fine grains of NaMgF₃ were isolated from an aqueous suspension and dried at 60 °C. The fine powder was loaded into diamond-anvil cells with 350 μm anvil culets. Tungsten was used to gasket the sample between the diamond anvils and graphite (1 wt%) was used to absorb the heating laser radiation. The sample was insulated from the anvils during heating using thin layers of NaCl, which also served as an internal pressure standard (Decker 1971; Sata et al. 2002).

Synchrotron X-ray diffraction experiments were conducted at the Advanced Photon Source (APS) at GeoSoilEnviroCARS (GSECARS) 13-ID-D, with $\lambda = 0.3344(2)$ Å, and at the High Pressure Collaborative Access Team (HPCAT) 16-ID-B, where $\lambda = 0.4018(2)$ Å. At the European Synchrotron Radiation Facility (ESRF) data were collected at ID-27 with $\lambda = 0.3738(2)$ Å. Beamline details are described previously for both GSECARS (Shen et al. 2005) and ID-27 (Mezouar et al. 2005). Data at HPCAT and ESRF were collected by a MAR345 imaging plate, while that at GSECARS was collected by a MAR CCD (2048 × 2048). Data were reduced using the program FIT2D (Hammersley et al. 1996) and any saturated pixels were excluded from the 360° (χ) intensity integration. The program EXPGUI (Toby 2001) for GSAS (Larson and Von Dreele 2000) was used for Rietveld structure modeling. The background, scale factor, and peak profile function type 3 (GW and LY only) amounted to seven variables.

The data presented in this paper were collected during separate runs and after double-sided infrared laser heating (Schultz et al. 2005). Data from pv-NaMgF₃ were collected after heating to temperatures of 2000 ± 200 K (Benedetti and Loubeyre 2004). To avoid high temperature phase transition in ppv-NaMgF₃ (Martin et al. 2006), this phase was not heated beyond 500 ± 200 °C. Because the Debye-Scherrer rings are round and not elliptical, we believe the variation in intensity around the rings results primarily from preferred orientation of sample powder, rather than from differential stress.

RESULTS

Rietveld structure refinement of pv-NaMgF₃ from monochromatic X-ray diffraction data indicate the atomic parameters, MgF₆ tilting angles (Zhao et al. 1993), and relative volumes of the A-site and B-site polyhedra (V_A/V_B ratio) (Thomas 1998) at 27(1) GPa just before the pv to ppv transition (Fig. 2a, Table 1a). The NaCl pressure media is present as both the B1 and B2 phases (Sata et al. 2002). In addition, we observe weak reflections (downward pointing arrows, Fig. 2a) in diffraction patterns above 14 GPa. The first 3 of these peaks at low angle may be indexed as the 022, 023, and 130 of ppv-NaMgF₃, which would confirm the phase requires a lower pressure to stabilize under shear stress (Liu et al. 2005). We believe the final 2 reflections at high angle

Post-perovskite structure models of NaMgF₃

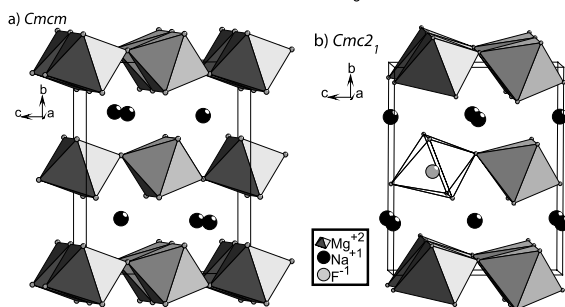


FIGURE 1. The orthorhombic post-perovskite structure of NaMgF₃ as (a) *Cmcm* and (b) *Cmc2*₁.

result from N-phase NaMgF₃ (Martin et al. 2006) rather than from graphite or unknown contamination. Our X-ray diffraction data (Martin et al. 2006) show a complete transformation of pv-NaMgF₃ (*Pbnm*) to ppv-NaMgF₃ above 27(1) GPa.

The X-ray diffraction data from ppv-NaMgF₃ show some evidence for non-uniform texture of the Debye-Scherrer rings and while portions show smooth intensity variation about changing angles of χ , there is evidence of sample recrystallization and/or reorientation close to 111_{*Cmcm*}. Our Rietveld refinements of ppv-NaMgF₃, using the CaIrO₃-type (*Cmcm*) structural model, assign too much intensity to the 020_{*Cmcm*} and 200_{*Cmcm*}, while assigning too little to the 002_{*Cmcm*} and 111_{*Cmcm*}. Texture due to preferred orientation of sample powder within the diamond-anvil cell may be modeled using a spherical-harmonic correction implemented in GSAS (Von Dreele 1997). However, the validity of this correction to in-situ high-pressure X-ray diffraction data of orthorhombic materials is debatable and in

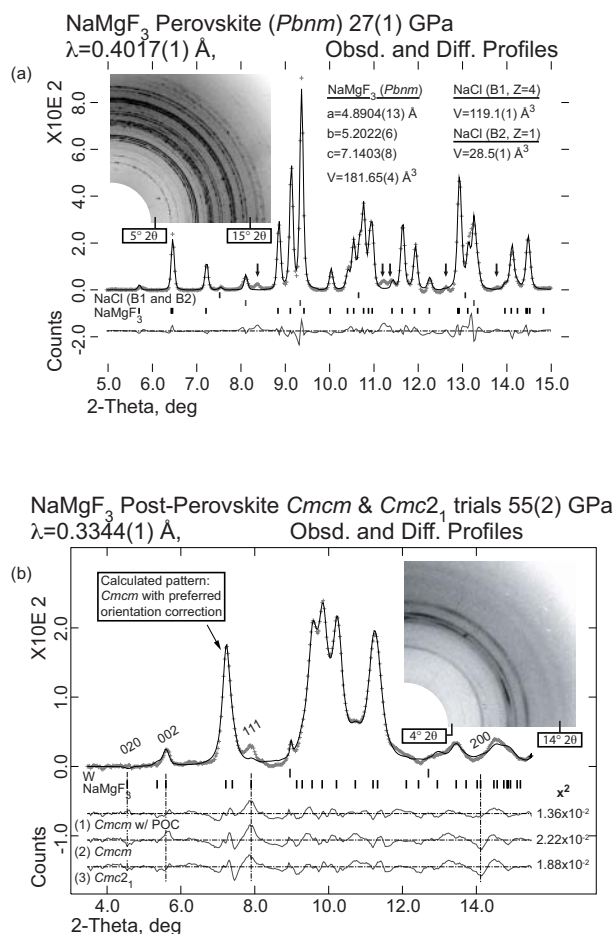


FIGURE 2. In-situ high pressure Rietveld structure modeling of (a) NaMgF₃ perovskite and (b) post-perovskite NaMgF₃. Portions of the raw two-dimensional data are inset in each plot to show sample texture. Difference curves of Rietveld structure models are plotted below the calculated (solid) and observed (dotted) background-subtracted X-ray diffraction patterns; (b) in descending order: (1) *Cmcm* with fourth-order spherical harmonic preferred orientation correction (POC), (2) *Cmcm* without POC, (3) *Cmc2*₁ without POC. Weak reflections marked with an arrow are indexed as NaMgF₃ post-perovskite.

practice, when carried out to more than four orders in this case, we find the spherical-harmonic correction will over-fit the data to the detriment of the structural model. While justification of the correction is difficult in this case, the correction may be checked by the texture index, a value summing the magnitude of each texture constant (Von Dreele 1997). Based on previous studies (Sitepu et al. 2005; Von Dreele 1997) and our own trials, we find the *Cmcm* structural model requires a cylindrical fourth-order spherical harmonic preferred orientation correction (cylindrical, 5 parameters) with a texture index of 2.14 (Fig. 2b and Table 1c) to achieve a satisfactory fit to the data.

Because it is not clear whether the intensity integration alone is sufficient to overcome effects of preferred orientation in the

data, we have investigated six non-isomorphic subgroups (I) of *Cmcm* (Hahn 1995) and observe a slightly better fit to diffraction patterns using an alternative structure model of ppv described by lower symmetry space group 36 (*Cmc2₁*, Fig. 1b) without a spherical harmonic texture correction. This model was investigated previously to describe a layered sulfide at room pressure (Wada and Onoda 1990), but was later refuted (Kim et al. 1997). This structure model allows extra degrees of freedom, amounting to displacement of B-site cations within further asymmetric BX₆ octahedra. Residuals from Rietveld refinement of *Cmc2₁* models are improved (Fig. 2b, Table 1d) and better fits to both 002_{*Cmc2₁*} and (200)_{*Cmc2₁*} are achieved, however some intensity of the 111_{*Cmc2₁*} as well as 200_{*Cmc2₁*} remain partially misfit. Rietveld structure models in the other subgroups, *C222₁* for example, improve the fit to 111, but are problematic with data at higher angle. Monoclinic models do not significantly improve the fit to the data nor suggest deviation from orthorhombic symmetry. While the data do not provide irrefutable evidence of a symmetry lower than the *Cmcm* (CaIrO₃) structural model for ppv-NaMgF₃, the distortion and asymmetry found in the *Cmc2₁* structure model could perhaps stabilize at extreme conditions. High-pressure studies on other compositions with the ppv structure, may help differentiate effects from preferred orientation.

DISCUSSION

The MgF₆ tilting angles and V_A/V_B ratio in the structure of pv-NaMgF₃ (*Pbnm*) at 27(1) GPa reveal an instability, which may drive structure transformation to ppv. The V_A/V_B ratio, an order parameter for perovskite-perovskite phase transitions, is 5 in cubic (*Pm3m*) perovskite structures and less than 5, though greater than 4, in perovskite structures where octahedra are tilted (Thomas 1998). At 27(1) GPa, the V_A/V_B value in pv-NaMgF₃ is 4.07(2), matching the V_A/V_B value observed in our Rietveld models of ppv-NaMgF₃ (*Cmcm*), 3.95(5). This ratio is also equal or close to 4 in the ppv-oxides MgSiO₃, 4.01, (Murakami et al. 2004), MgGeO₃, 4.28, (Hirose et al. 2005), CaIrO₃, 4.19, (Rodi and Babel 1965), and Fe₂O₃, 3.89, (Ono and Ohishi 2005). This realization is significant because it suggests minimal relative reconstruction of each site is required to transition from pv to ppv. In addition, it may be possible to predict the pressure of a pv-ppv phase transition in other perovskite (or A₂X₃) structured materials by extrapolating the change in V_A/V_B at high pressure to a value close to 4. Combining previous data (Liu et al. 2005) with our current results, we find that V_A/V_B for pv-NaMgF₃ decreases linearly with pressure at a rate of 1.40(2) × 10⁻² GPa⁻¹ between 1 bar and 27(1) GPa.

Examination of the Rietveld structure model of pv-NaMgF₃ at 27(1) GPa reveals that tilting of the perovskite octahedra (Glazer 1972; Liu et al. 2005; Thomas 1998) forces some extra-octahedral F-F distances to rival the average intra-octahedral F-F distance. At which point electrostatic repulsion between select pairs of extra-octahedral fluorine atoms may strain the pv octahedral unit enough to drive the transition to ppv structure. The most notable difference between MgF₆ octahedra in pv and ppv is the amount of strain. Octahedra in ppv-NaMgF₃, as well as the published CaIrO₃-type oxides, demonstrate twice the average value of shear strain (via strain matrix, see Zhao et al. 1993) as that observed for pv-NaMgF₃. This significant strain observed

TABLE 1. Structure parameters derived from Rietveld refinement of data for (a) NaMgF₃ perovskite at 27(1) GPa, (b) post-perovskite structure models of NaMgF₃ at 54(2) GPa without correction for preferred orientation as *Cmcm*, (c) with correction for preferred orientation as *Cmcm*, and (d) without correction for preferred orientation as *Cmc2₁*.

(a)					
	a (Å)	b	c	V (Å³)	
	4.8904(13)	5.2022(6)	7.1403(8)	181.65(4)	
	Na (4c)	Mg (4b)	F1 (4c)	F2 (8d)	
x	0.9771(19)	0.0000	0.1019(25)	0.6750(17)	
y	0.0802(13)	0.5000	0.4697(17)	0.3110(10)	
z	0.2500	0.0000	0.2500	0.0619(12)	
Octahedra Tilt					
	φ (°)		θ (°)		Φ (°)
	15.2(8)		17.8(7)		23.2(6)
Mg-F1 (x2)	Mg-F2 (x2)	Mg-F2 (x2)	V_b (Å³)	V_A/V_B (Å³)	
1.860(4)	1.886(7)	1.917(8)	8.95(8)	4.07(5)	
Residuals	χ²	wRp	R(F²)		Dwd
MAR345 (IP)	0.1190	0.0098	0.0588		0.5810
(b)					
	a (Å)	b	c	V (Å³)	
	2.7145(14)	8.393(5)	6.8512(23)	156.09(7)	
	Na (4c)	Mg (4a)	F1 (4c)	F2 (8f)	
x	0.0000	0.0000	0.5000	0.5000	
y	0.2567(13)	0.0000	0.4242(15)	0.1402(8)	
z	0.2500	0.0000	0.2500	0.0676(12)	
Mg-F1 x2	Mg-F2 x4	V_b (Å³)	V_A/V_B (Å³)		
1.827(5)	1.855(6)	8.36(1)	3.66(8)		
Residuals	χ²	wRp	R(F²)		Dwd
MAR CCD	0.0222	0.0038	0.0325		0.1120
(c)					
	a (Å)	b	c	V (Å³)	
	2.7164(16)	8.381(5)	6.8487(25)	155.9(1)	
	Na (4c)	Mg (4a)	F1 (4c)	F2 (8f)	
x	0.0000	0.0000	0.5000	0.5000	
y	0.2422(14)	0.0000	0.4433(12)	0.1385(10)	
z	0.2500	0.0000	0.2500	0.0579(9)	
Preferred orientation constants from GSAS. Texture Index = 2.1429. C_i^{nm} as (l,m,n)					
(2,0,0)	(2,0,2)	(4,0,0)	(4,0,2)	(4,0,4)	
-1.1883	0.3942	-0.3545	-1.6891	-2.1180	
Mg-F1 x2	Mg-F2 x4	V_b (Å³)	V_A/V_B (Å³)		
1.777(3)	1.830(6)	7.881(82)	3.94(6)		
Residuals	χ²	wRp	R(F²)		Dwd
MAR CCD	0.0136	0.0030	0.0196		0.1480
(d)					
	a (Å)	b	c	V (Å³)	
	2.7143(9)	8.393(3)	6.846(2)	155.99(9)	
	Na (4a)	Mg (4a)	F1 (4a)	F2 (4a)	F3 (4a)
x	0.0000	0.0000	0.0000	0.0000	
y	0.2531(6)	0.0129(13)	0.9251(7)	0.6286(10)	
z	0.0036(7)	0.2556(18)	0.0000(7)	0.1551(9)	
Mg-F1a	Mg-F1b	Mg-F2 x2	Mg-F3	V_b (Å³)	V_A/V_B (Å³)
1.900(15)	1.752(15)	1.805(10)	1.975(10)	8.44(1)	3.62(5)
Residuals	χ²	wRp	R(F²)		Dwd
MAR CCD	0.0188	0.0035	0.0325		0.1310

Note: V_A/V_B ratio was calculated considering, V_A = (V_{UC}/Z) - V_b.

of octahedra in CaIrO₃-type structures (Rodi and Babel 1965) is likely not favored by the B-site cation and may help explain why so few CaIrO₃-type structures are stable at room pressure. Similarly, shear strain of octahedra in ppv-NaMgF₃ likely contributes to instability in the structure, which transforms to an unknown orthorhombic phase upon laser heating (Martin et al. 2006).

ACKNOWLEDGMENTS

This work was supported by grant NSF-EAR-0510501 to J.B.P. and we acknowledge the ESRF for provision of beamtime to proposal number HS-2780 at ID-27. Portions of this work were performed at GeoSoilEnviroCARS (Sector 13) as well as HPCAT (Sector 16), Advanced Photon Source (APS), Argonne National Laboratory. GeoSoilEnviroCARS is supported by the National Science Foundation—Earth Sciences (EAR-0217473), Department of Energy—Geosciences (DE-FG02-94ER14466) and the State of Illinois. Use of the HPCAT facility was supported by DOE-BES, DOE-NNSA (CDAC), NSF-DOD-TACOM, and the W.M. Keck Foundation. Use of the APS was supported by the U.S. Department of Energy, Office of Science, Office of Basic Energy Sciences, under contract no. W-31-109-ENG-38. Two anonymous reviewers gave thoughtful comments and corrections that improved this work.

REFERENCES CITED

- Benedetti, L.R. and Loubeyre, P. (2004) Temperature gradients, wavelength-dependent emissivity, and accuracy of high and very-high temperatures measured in the laser-heated diamond cell. *High Pressure Research*, 24, 423–445.
- Caracas, R. and Cohen, R.E. (2005) Effect of chemistry on the stability and elasticity of the perovskite and post-perovskite phases in the MgSiO₃-FeSiO₃-Al₂O₃ system and implications for the lowermost mantle. *Geophysical Research Letters*, 32, L16310, DOI:10.1029/2005GL023164.
- Chao, E.C.T., Evans, H.T., Skinner, B.J., and Milton, C. (1961) Neighborite, NaMgF₃, a New Mineral From the Green River Formation, South Ouray, Utah. *American Mineralogist*, 46, 379–393.
- Decker, D.L. (1971) High-Pressure Equation of State for NaCl, KCl, and CsCl. *Journal of Applied Physics*, 42, 3239.
- Duffy, T.S., Kubo, A., Shieh, S.R., Shen, G.Y., Prakapenka, V.B., Kiefer, B., and Shim, S.H. (2005) Compressibility and Structural Evolution of Germanate and Silicate Post-Perovskite Phases. *AGU Fall Meeting 2005 No. MR22A-07*.
- Dziewonski, A.M. and Anderson, D.L. (1981) Preliminary Reference Earth Model. *Physics of the Earth and Planetary Interiors*, 25, 297–356.
- Garnero, E.J. (2004) A new paradigm for Earth's core-mantle boundary. *Science*, 304(5672), 834–836.
- Glazer, A.M. (1972) Classification of Tilted Octahedra in Perovskites. *Acta Crystallographica Section B—Structural Science*, B 28, 3384–3392.
- Hahn, T. (1995) *International Tables for Crystallography, Vol. A, SpaceGroup Symmetry*. Kluwer Academic Publishers, Dordrecht.
- Hammersley, A.P., Svensson, S.O., Hanfland, M., Fitch, A.N., and Häusermann, D. (1996) Two-dimensional detector software: From real detector to idealized image or two-theta scan. *High Pressure Research*, 14, 235–248.
- Hirose, K. and Fujita, Y. (2005) Clapeyron slope of the post-perovskite phase transition in CaIrO₃. *Geophysical Research Letters*, 32, L13313, DOI: 10.1029/2005GL023219.
- Hirose, K., Kawamura, K., Ohishi, Y., Tateno, S., and Sata, N. (2005) Stability and equation of state of MgGeO₃ post-perovskite phase. *American Mineralogist*, 90, 262–265.
- Karato, S.-I. and Karki, B.B. (2001) Origin of lateral variation of seismic wave velocities and density in the deep mantle. *Journal of Geophysical Research*, 106, 21771–21784, DOI: 10.1029/2001JB000214.
- Kim, C., Yun, H.S., Lee, Y., Shin, H., and Liou, K. (1997) Structure and electrical conductivity of AgTaS₃. *Journal of Solid State Chemistry*, 132, 389–393.
- Larson, A.C. and Von Dreele, R.B. (2000) *General Structure Analysis System (GSAS)*. Los Alamos National Laboratory Report, 86-748.
- Lay, T., Williams, Q., and Garnero, E.J. (1998) The core-mantle boundary layer and deep Earth dynamics. *Nature*, 392, 461–468.
- Lay, T., Garnero, E.J., and Williams, Q. (2004) Partial melting in a thermo-chemical boundary layer at the base of the mantle. *Physics of the Earth and Planetary Interiors*, 146, 441–467.
- Liu, H.-Z., Chen, J., Hu, J., Martin, C.D., Weidner, D.J., Häusermann, D., and Mao, H.-K. (2005) Octahedral tilting evolution and phase transition in orthorhombic NaMgF₃ perovskite under pressure. *Geophysical Research Letters*, 32, L04304, DOI: 10.1029/2004GL022068.
- Mao, L.W., Mao, H.K., Sturhahn, W., Zhao, J., Prakapenka, V.B., Meng, Y., Shu, J.F., Fei, Y.W., and Hemley, R.J. (2006) Iron-Rich Post-Perovskite and the Origin of Ultralow-Velocity Zones. *Science*, 312, 564–565.
- Martin, C.D., Chaudhuri, S., Grey, C.P., and Parise, J.B. (2005) Effect of A-site cation radius on ordering of BX₆ octahedra in (K,Na)MgF₃ perovskite. *American Mineralogist*, 90, 1522–1533.
- Martin, C.D., Crichton, W.A., Liu, H., Prakapenka, V., Chen, J., and Parise, J.B. (2006) Phase transitions and compressibility of NaMgF₃ (Neighborite) in perovskite- and post-perovskite-related structures. *Geophysical Research Letters*, 33, L11305, DOI: 10.1029/2006GL026150.
- Mezour, M., Crichton, W.A., Bauchau, S., Thurel, F., Witsch, H., Torrecillas, F., Blattmann, G., Marion, P., Dabin, Y., Chavanne, J., Hignette, O., Morawe, C., and Borel, C. (2005) Development of a new state-of-the-art beamline optimized for monochromatic single-crystal and powder X-ray diffraction under extreme conditions at the ESRF. *Journal of Synchrotron Radiation*, 12, 659–664.
- Murakami, M., Hirose, K., Kawamura, K., Sata, N., and Ohishi, Y. (2004) Post-perovskite phase transition in MgSiO₃. *Science*, 304, 855–858.
- Murakami, M., Hirose, K., Sata, N., and Ohishi, Y. (2005) Post-perovskite phase transition and mineral chemistry in the pyrolytic lowermost mantle. *Geophysical Research Letters*, 32, L03304, DOI: 10.1029/2004GL021956.
- Oganov, A.R. and Ono, S. (2004) Theoretical and experimental evidence for a post-perovskite phase of MgSiO₃ in Earth's D" layer. *Nature*, 430, 445–448.
- O'Keefe, M., Hyde, B.G., and Bovin, J.O. (1979) Contribution to the Crystal-Chemistry of Orthorhombic Perovskites—MgSiO₃ and NaMgF₃. *Physics and Chemistry of Minerals*, 4, 299–305.
- Ono, S. and Ohishi, Y. (2005) In situ X-ray observation of phase transformation in Fe₂O₃ at high pressures and high temperatures. *Journal of Physics and Chemistry of Solids*, 66, 1714–1720.
- Parise, J.B., Umemoto, K., Wentzcovitch, R.A., and Weidner, D.J. (2004) Post-perovskite transition in NaMgF₃. *AGU Fall Meeting 2004 No. MR23A-0188*.
- Rodi, F. and Babel, D. (1965) Ternäre Oxide Der Übergangsmetalle. 4. Erdalkali-iridium(4)-Oxide-Kristallstruktur Von CaIrO₃. *Zeitschrift für Anorganische und Allgemeine Chemie*, 336, 17–23.
- Santillan, J. and Shim, S.H. (2005) High Pressure Phase transition in Mn₂O₃ to the CaIrO₃-type Phase. *AGU Fall Meeting 2005 No. MR23B-0050*.
- Sata, N., Shen, G.Y., Rivers, M.L., and Sutton, S.R. (2002) Pressure-volume equation of state of the high-pressure B2 phase of NaCl. *Physical Review B*, 65, DOI: 10.1103/PhysRevB.65.104114.
- Schultz, E., Mezour, M., Crichton, W., Bauchau, S., Blattmann, G., Andrault, D., Fiquet, G., Boehler, R., Rambert, N., Sitaud, B., and Loubeyre, P. (2005) Double-sided laser heating system for in situ high pressure-high temperature monochromatic X-ray diffraction at the ESRF. *High Pressure Research*, 25, 71–83.
- Shen, G.Y., Prakapenka, V.B., Eng, P.J., Rivers, M.L., and Sutton, S.R. (2005) Facilities for high-pressure research with the diamond anvil cell at GSECARS. *Journal of Synchrotron Radiation*, 12, 642–649.
- Shieh, S.R., Duffy, T.S., Kubo, A., Shen, G.Y., Prakapenka, V.B., Sata, N., Hirose, K., and Ohishi, Y. (2006) Equation of state of the postperovskite phase synthesized from a natural (Mg,Fe)SiO₃ orthopyroxene. *Proceedings of the National Academy of Sciences of the United States of America*, 103, 3039–3043.
- Sitepu, H., O'Connor, B.H., and Li, D. (2005) Comparative evaluation of the March and generalized spherical harmonic preferred orientation models using X-ray diffraction data for molybdenite and calcite powders. *Journal of Applied Crystallography*, 38, 158–167.
- Tateno, S., Hirose, K., Sata, N., and Ohishi, Y. (2006) High-pressure behavior of Mn-GeO₃ and CdGeO₃ perovskites and the post-perovskite phase transition. *Physics and Chemistry of Minerals*, 32, 721–725.
- Thomas, N.W. (1998) New global parameterization of perovskite structures. *Acta Crystallographica Section B—Structural Science*, 54, 585–599.
- Toby, B.H. (2001) EXPGUI, a graphical user interface for GSAS. *Journal of Applied Crystallography*, 34, 210–213.
- Tsuchiya, T., Tsuchiya, J., Umemoto, K., and Wentzcovitch, R.A. (2004) Phase transition in MgSiO₃ perovskite in the earth's lower mantle. *Earth and Planetary Science Letters*, 224, 241–248.
- Von Dreele, R.B. (1997) Quantitative texture analysis by Rietveld refinement. *Journal of Applied Crystallography*, 30, 517–525.
- Wada, H. and Onoda, M. (1990) Preparation of New Compound AgTaS₃. *Chemistry Letters*, 5, 705–706.
- Zhao, Y.S., Weidner, D.J., Parise, J.B., and Cox, D.E. (1993) Thermal-Expansion and Structural Distortion of Perovskite-Data For NaMgF₃ Perovskite. 1. *Physics of the Earth and Planetary Interiors*, 76, 1–16.

MANUSCRIPT RECEIVED MAY 10, 2006

MANUSCRIPT ACCEPTED JUNE 14, 2006

MANUSCRIPT HANDLED BY BRYAN CHAKOUMAKOS